Fragmentation of leucine-enkephalin by collision induced dissociation for different keV projectile ions

M. Door

Bachelor thesis in physics

September 2009

KVI, Rijksuniversiteit Groningen

Supervisors: prof. dr. ir. R. Hoekstra, dr. T. Schlathölter and drs. S. Bari

Abstract

It is still unexplored how keV ions interact with isolated DNA molecules and into which fragments the DNA eventually dissociates. Such knowledge is important for the improvement of proton (tumor) therapy since DNA damage is one of the basic mechanism underlying biological radiation damage. Experiments on ion induced dissociation are performed with the new Paultje setup at the Kernfysisch Versneller Instituut (KVI) of the Rijksuniversiteit of Groningen. This bachelor thesis describes the experimental setup and performed experiments which are subsequently analyzed. In our experiments Leucine-enkephalin, a penta-peptide also found in humans, is irradiated with He^{q+} ions of different charge state and velocity.

Contents

Chapter 1

Introduction and motivation

Most of the biological radiation damages are attributable to damaged DNA. Healthy tissue must be protected against this ionizing radiation which originates from e.g. radioactive elements in the environment or nuclear medicine diagnostics. The DNA is a double-stranded macromolecule. It consists of nucleotides, which are made of sugar and phosphate groups (the backbones of a strand), and bases, which carry the genetic information (see fig.1). Bases of the DNA are Adenine, Cytosine, Thymine and Guanine.

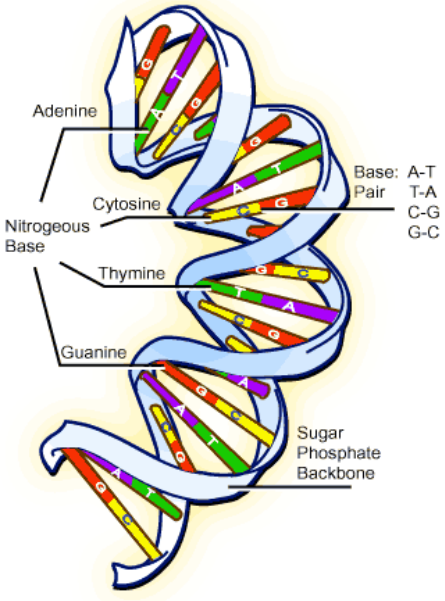

Fig.1: A general overview of the DNA [1].

Exposed to ionizing radiation, DNA can suffer from Single Strand Breaks (SSBs), Double Strand Breaks (DSBs) or clustered lesions. SSBs can be repaired with a high probability, which results in a healthy cell. But also mis-repair leading to mutation or even cell death can occur. DSBs are repaired with a lower probability, because of the larger damage and the lack of the intact complementary strand. Mis-repair, mutations and cell death are more frequent. There is a theory of so-called clustered lesions (irreparable damage of the DNA), which occur when DNA is damaged at close together lying locations by direct and indirect damage [2]. Note that this theory is not proven yet.

Radiation damage is of course undesired with regard to healthy tissue. But in cancer therapy, the use of ionizing radiation (ion therapy) is a promising technique to destroy tumors even located far within the body or the head.

1.1 Radiation therapy in comparison with ion therapy

In radiation therapy, X-Rays, γ-radiation and electrons are used. The main difference of these kinds of ionizing radiation is the difference in their linear energy transfers (LET). Ions have a high LET compared to photons, this means that they transfer a lot more energy per unit of length to the medium than photons. The consequence is that ions stop inside the medium losing their ultimate rest of energy (Bragg-peak), while photons still have enough energy to pass out the medium. As one can see in fig.2, the maximum relative doses in water (comparable with the maximum relative doses in human tissue) are reached at approximately 1 cm ^{60}Co γ-rays (in the order of 1 keV) and 3 cm for high energy photons (18 MeV). In these depths, the kinds of radiations have their maximum effects. X-Rays penetrating in tissue lose their energy exponentially. In cancer therapy, the main disadvantage is that the energy is not solely given to the tumor, but also to healthy tissue in front of it. This holds true for photons and γ-rays, too. The only difference is that a large percentage is given to the healthy tissue behind the tumor.
The usage of ions in tumor therapy has a tremendous advantage. Entering the tissue, the ions are still fast and deliver just a little bit of their energy to the healthy tissue. Reaching a critical velocity in a certain depth (where the tumor is), the energy deposition becomes large. Fig.2 shows this phenomenon which is known as the Bragg-peak (^{12}C-ions: ~4 GeV). The position of the Bragg-peak can be controlled by changing the primary ion beam energy. In this way, the healthy tissue is only weakly damaged in front of the tumor and spared behind, while the tumor experiences the majority of the ion energy [2].

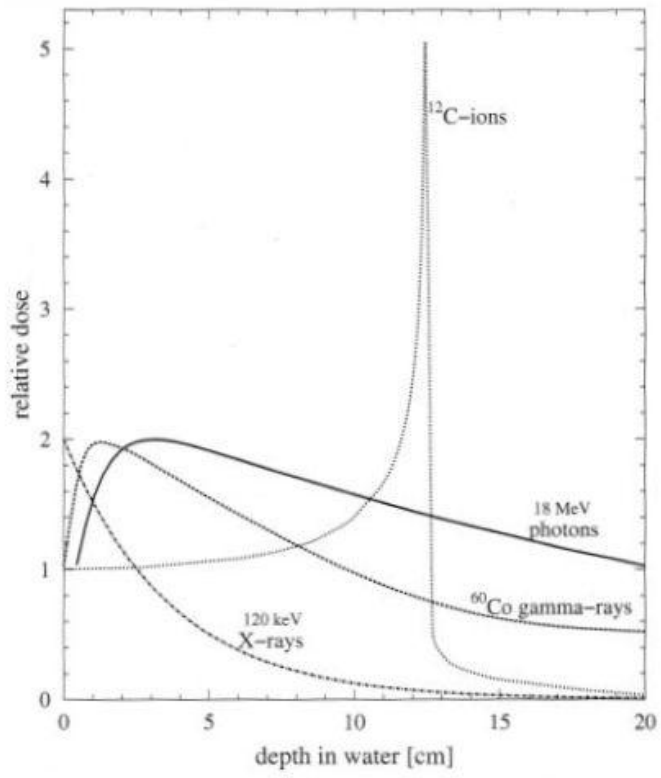

Fig.2: the depth-dose distribution of photons, X-Rays, γ-rays and 12C-ions [2].

Chapter 2

Experimental Setup

In the Paultje setup, a solution of the molecule of interest is ionized by electrospray ionization (ESI). By several lenses and two quadrupole mass filters, ions are pre-selected with respect to their mass and trapped in a Paul trap. In the Paul trap, the ionized molecules are irradiated with ions extracted from the electron cyclotron resonance ion source (ECRIS). A fraction of the ions dissociate due to ion-molecule collisions. The resulting ion cloud is extracted from the Paul trap and subsequently guided through a time of flight mass spectrometer (TOFMS). In this way, the ion yield as a function of ion mass is observed. With the computer program OriginPro, measured data are processed and spectra are plotted.

In this chapter, the components of the experimental setup will be discussed in more detail.

2.1 Electrospray Ionization

Electrospray ionization (ESI) is a method to produce macromolecular ions from solution, e.g. in order to perform mass spectrometry. J.B. Fenn received the Nobel Prize in Chemistry for “the development of methods for identification and structure analyses of biological macromolecules” in 2002. ESI is convenient for macromolecules, because at the end of the ionization process, they have a low internal energy, so that the ions stay intact and do not fragment during their production. This is ideal for the Paultje experiment, because of the aim to trap intact molecules in order to look at the fragmentation due to collisions with keV ions.

How it works

A solution of the molecule of interest (analyte) dissolved in methanol and/or water (solvent) enters the ES chamber through a stainless steel needle (flow rates 1-20µl/min), biased to a voltage of the order of a few kV relative to the ES chamber and to the cylindrical electrode. This voltage difference is responsible for the fine nebulization and for the ionization of the analyte.

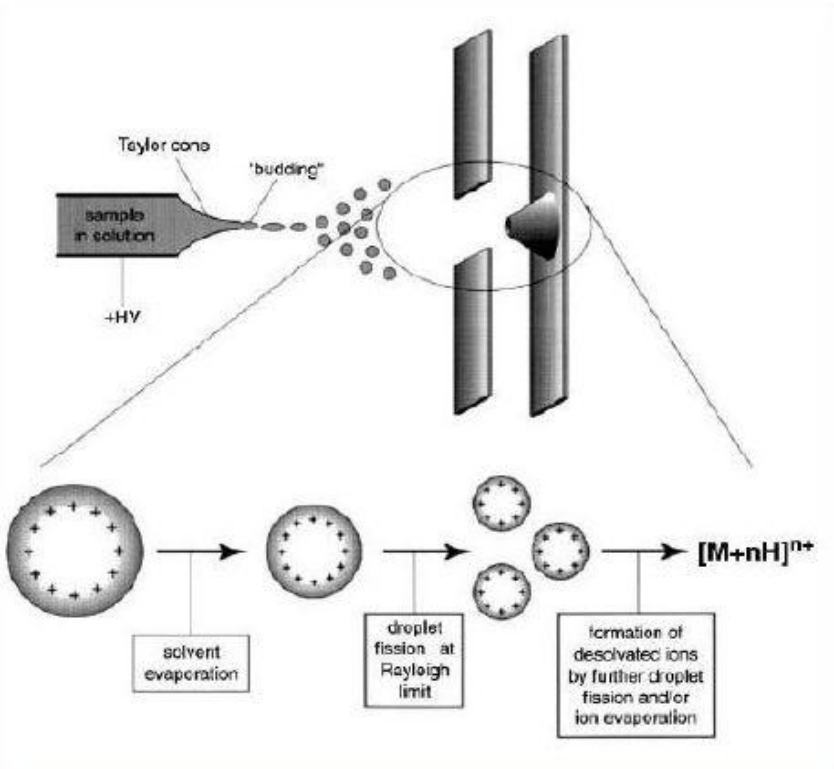

Fig.2.1: Formation of the Taylor Cone and the nebulization process [3].

In a little bit more detail, the nebulization works as follows: At the needle tip, the liquid droplet experiences charge separation by the electric field which is present there. Solely positive or negative charges are located at the droplets surface (depending on the polarization of the voltage), which repel each other. This results in a so called Taylor cone (fig.2.1). The form of the Taylor cone depends on the balance of the strength of the electric field and the surface tension of the liquid. When a certain distance to the end of the needle is reached, the cone becomes instable and emits a charged spray, the cone jet.

Due to the electric field, the spray of small droplets moves to the inlet of the heated (~140°C) capillary (see fig.2.2, which is an illustration of a setup for another system). The capillary is oriented off-axis, so that unwanted neutral molecules hit the walls of the capillary. Note that there is no drying gas used in the Paultje setup.

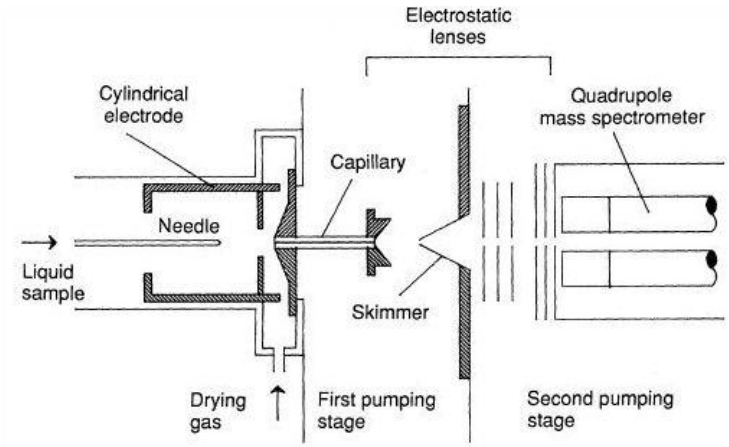

Fig.2.2: The stages of the droplets in electrospray ionization [4].

In the capillary, the decreasing radius of the droplets implicates an increasing charge density on their surfaces. The charge density is limited by the Rayleigh limit: Droplets in a gas can accommodate only a certain, limited number of the same charges, which depends on the radius of the droplets and the surface tension. When the Rayleigh limit is reached, the droplets become unstable and "explode" (often called "Coulomb explosion"). In this way, charged daughter droplets are formed, whose remaining solvent also evaporates. The radius of the daughter droplets minimizes and when the surface charge density is strong enough, ions are desorbed from the droplet to the ambient gas.

The ions exit the capillary as a supersonic free jet off-axis into the first vacuum chamber. A fraction of the ions is forced by the surrounding tube lens onto the source axis and passes the skimmer into the second vacuum chamber. Note that the off-axis orientation of the capillary and the tube lens are not illustrated in fig.2.2. The voltage of the skimmer helps focusing the analyte ions. The ions pass an ion guide, which focuses the ions by collisions (collisional focusing). After that, ions are ready to be guided through e.g. a mass filter.

There is disagreement about the ion desorption process. The process has not been proved yet, and there are two theories about it. The first is the charge residue model (CRM). It conveys that tiny droplets of about 1nm diameter remain, containing one ionized analyte molecule. The second theory is the ion evaporation model (IEM). The idea of the IEM is that free ions are directly emitted to the ambient gas from larger charged droplets. A negligible loss of mass, but a large drop of charge occurs to the droplet. These ions are directed to the mass filter by the present electric field between the needle and the orifice [3], [4], [5].

2.2 Linear Quadrupole mass spectrometer (mass filter)

In 1953, Wolfgang Paul and Helmut Steinwedel developed the linear quadrupole mass spectrometer [6]. It separates ions with respect to their masses with the aid of a high frequency electric field. The mass filter consists of a set of four hyperbolically shaped metal rods, which act as electrodes (fig.2.3a). For further calculations they are chosen to be placed in the y-direction. The electrode-pairs opposite to each other are connected to a 180 degrees phase shifted r.f.-potential in addition to a dc potential:

$$\phi = U + V\cos(\Omega t) \qquad (2.1)$$

The resulting inhomogeneous electric field is shown in fig.2.3b. By either variation of the voltages U and V and keeping the frequency constant, or variation of the frequency and keeping U and V constant the range of masses passing the filter can be changed.

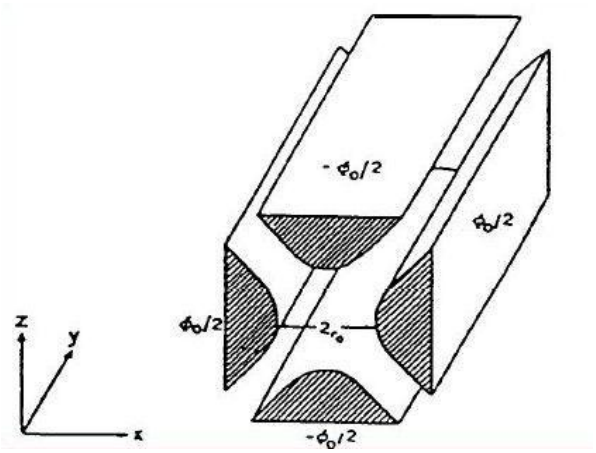

Fig.2.3a: The four metal rods of the quadrupole mass spectrometer (in y-direction) with the applied voltage and the distance between two electrodes [6].

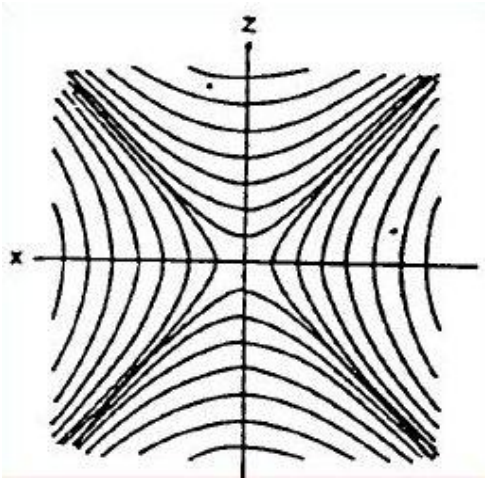

Fig.2.3b: The equipotential fieldlines of the electric field between the electrodes [6].

Ions entering the quadrupole field will be focused and defocused in both the x- and z-directions alternating in time. The reason for this is the periodically applied voltage V. Only particles with a certain mass-to-charge ratio m/z traverse the quadrupole by oscillating paths without hitting the electrodes. Too heavy or too light ions hit the electrodes and discharge. This can also be shown by the following calculations, which are given concisely here (see appendix for the full elaboration):

The stated below Mathieu-equation describes the motion of an ion through a quadrupole mass filter:

$$\frac{d^2u}{d\xi^2} = [a_u - 2q_u\cos(2\xi)]u = 0 \qquad (2.2)$$

With a_u and q_u the dimensionless trapping parameters, $\xi = \frac{\Omega t}{2}$ with Ω the angular frequency of the r.f.-field and u a variable, which can be replaced by x or z for the x- and z-direction, respectively. Note that the y-direction is not taken into account here, because this is the moving direction of the ions parallel to the rods, while the electric field is 2-dimensional in the xz-direction. The ions experience no force in the y-direction by the quadrupole field.

Substituting ξ, multiplying with the ion mass m and rearranging modifies equation 2.2 in

$$m\frac{d^2u}{dt^2} = -\frac{\Omega^2}{4}m(a_u - 2q_u\cos(\Omega t))u \qquad (2.3)$$

Note that the left-handed side represents the force on an ion in the u-direction.

The potential in a quadrupole is given by

$$\phi = \frac{\phi_0}{2r_0^2}(\lambda x^2 + \sigma y^2 + \gamma z^2) \qquad (2.4)$$

With r_0 half the distance between two opposite electrodes and λ, σ and γ symbolize weighting constants for the x-, y- and z-directions, respectively. For a mass filter, $\lambda = -\gamma = 1$ and $\sigma = 0$ since there is no focusing force in the y-direction. Equation 2.4 reduces to

$$\phi = \frac{\phi_0}{2r_0^2}(x^2 - z^2) \qquad (2.5)$$

Taking the derivative with respect to x and substituting eq. 2.1, the force on an ion in the x-direction is calculated as

$$F_x = -e\frac{\partial\phi}{\partial x} = -e\frac{x}{r_0^2}\big(U + Vcos(\Omega t)\big) \qquad (2.6)$$

Equations 2.3 and 2.6 both represent forces on an ion. Replacing u by x in equation 2.3, comparing it with equation 2.6 and rearranging the formulas, the trapping parameters can be expressed as

$$a_x = \frac{4eU}{mr_0^2\Omega^2} \qquad and \qquad q_x = -\frac{2eV}{mr_0^2\Omega^2} \qquad (2.7)$$

$$\Leftrightarrow\ U = \frac{m}{e}\frac{a_x r_0^2\Omega^2}{4} \qquad and \qquad V = -\frac{m}{e}\frac{q_x r_0^2\Omega^2}{2} \qquad (2.8)$$

Because of the weighting constants $\lambda = -\gamma = 1$, the trapping parameters for the z-direction are deemed to be

$$a_z = -a_x \qquad and \qquad q_z = -q_x \qquad (2.8)$$

The values for a_u and q_u originate from the Mathieu-equation (eq. 2.2) and are obtained by solving it. In a plot of a_u as a function of q_u, there are regions of stable motion for the x- and z-directions. This stability diagram is shown in fig.2.4a. Certainly, the motion of the ions has to be stable in both the x- and z-direction, so one has to take a closer look at the part where x-stable and z-stable solutions overlap (fig.2.4b). It can easily been read off that on the q-axis this is the case for $(a, q) = (0\,, 0.92)$. All ion masses lie on the operation line, as indicated in the figure [6].

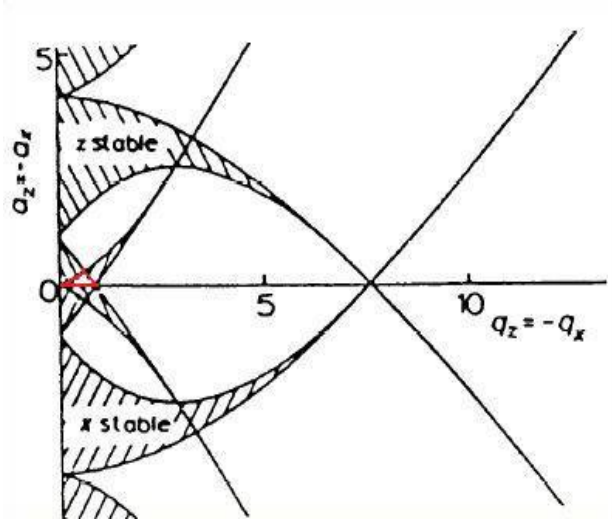

Fig.2.4a: The overall stability diagram for the 2-dimensional Quadrupole field of the mass filter [6].

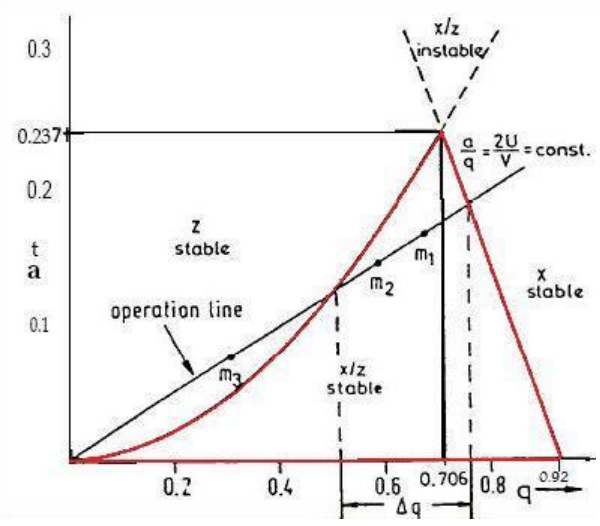

Fig.2.4b: simultaneous stability in the x- and z-direction within the red labeling [6].

2.3 Paul Trap (Quadrupole ion trap)

As the name implies, this device is also invented by Wolfgang Paul, for which he received the Nobel prize in 1989. Different to the 2-dimensional field in the linear mass spectrometer, an ion trap makes use of a 3-dimensional field. The Paul trap is built by a hyperbolical shaped ring electrode and two rotationally hyperbolic end-cap electrodes, as shown in fig.2.5a and b. All relevant parameters are indicated in the figure.

Fig. 2.5a: The cross-section of a Paul trap. In the middle is the ring electrode, above and below the en cap electrodes [7].

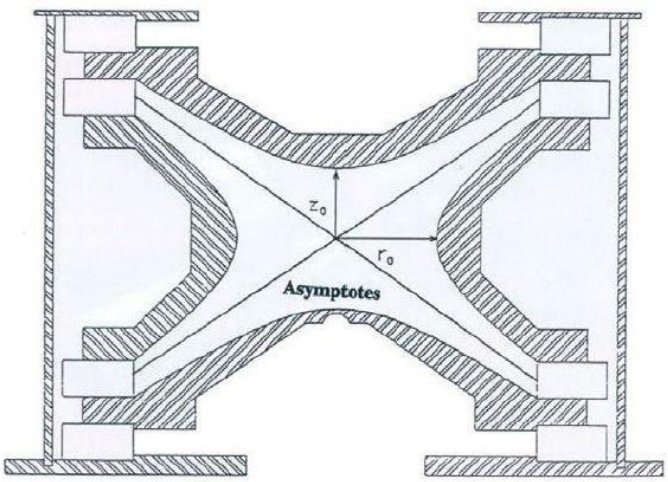

Fig. 2.5b: The same viewing direction as in figure 3a, with the parameters z_0 and r_0 [7].

Ions in the trap obey the same motion as in the mass filter, but the electric field in the z-direction is two times stronger compared to a mass filter, because $2z_0{}^2 = r_0{}^2$. The weighting constants are thus $\lambda = \sigma = 1$ and $\gamma = -2$. Again, a periodically applied voltage $\phi = U + Vcos(\Omega t)$) is required to stabilize the path of the ions. The arising electric field is shown in fig.2.6:

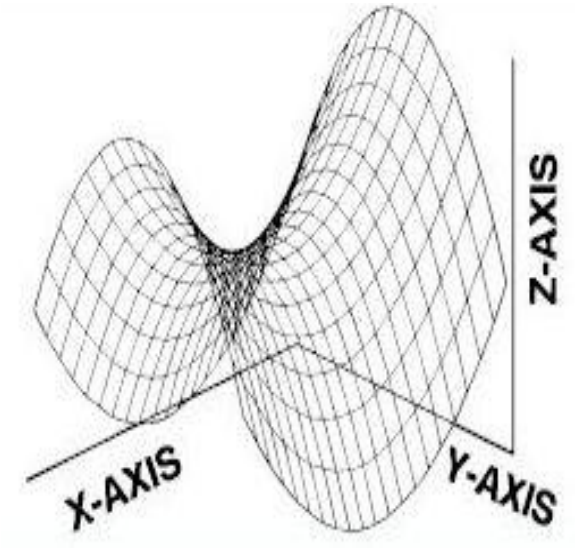

Fig.2.6: Potential surface of quadrupole ion trap [7].

It is a notable illustration to the idea of the mechanical analogue by W.Paul: "In the trap the equipotential lines form a saddle surface (...). We have machined such a surface on a round disc. If one puts a small steel ball on it, then it will roll down: its position is unstable. But if one let the disk rotate with the right frequency appropriate to the potential parameters and the mass of the ball, the ball becomes stable, makes small oscillations and can be kept in position over a long time. Even if one adds a second or a third ball they stay near the center of the disc. The only condition is that the related Mathieu parameter q be in the permitted range." ([6], p.610)

The trapping (Mathieu) parameters a_u and q_u can be found in a similar manner than for the mass filter. Additionally, one will attain the same results (see eq.2.7). For the ion trap, $\lambda = \sigma = 1$, so $a_x = a_y$ and $q_x = q_y$.

The trapping parameters for the z-direction ($\gamma = -2$) are given by

$$a_z = -8\frac{eU}{r_0 m\Omega^2} \qquad and \qquad q_z = 4\frac{eV}{r_0 m\Omega^2} \qquad (2.10)$$

The full calculation is left out here, but checkable in the appendix.

The stability diagram for the Paul trap is shown in fig.2.7:

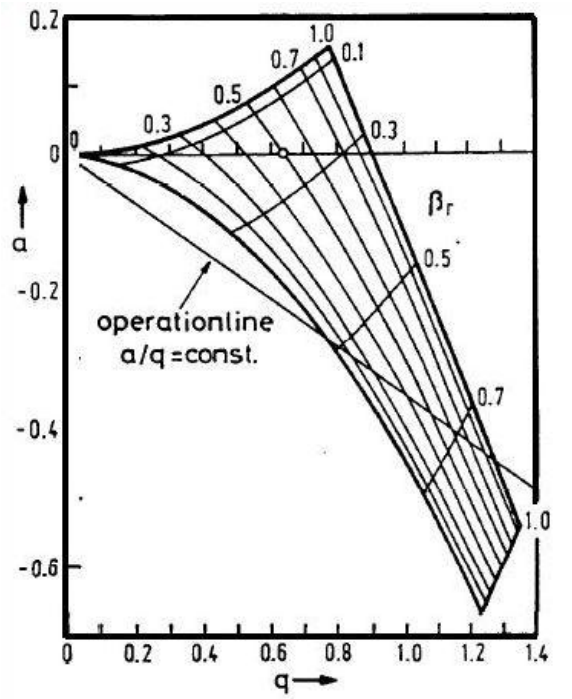

Fig.2.7 stability diagram of the Paul trap [6]

Because of the different weighting constant in the z-direction, this stability diagram is different to that of the mass filter. All ion masses lie on the operation line $\frac{a}{q} = \frac{2U}{V}$. Near the q-axis, the ion motions are most stable. This situation can be achieved by lowering the dc voltage.

In the Paultje experiment, ions in the Paul trap have a larger kinetic energy than allowed by the potential surface (a few eV). As a result, the ions can not be trapped. They have to be cooled down (lower the kinetic energy) by a buffer gas (helium), so that the trajectories become narrower and the ions can be trapped. Helium is used because it has the highest ionization energy and consequently exchanges only kinetic energy and no charge with the ionized molecules in the Paul trap. After being cooled down, the molecules are supposed to be irradiated with the ions extracted from the ECRIS. Therefore, a low pressure is provided, that means that the buffer gas has to be extracted from the Paul trap before irradiation. This is why the buffer gas in the ion trap has to be pulsed [6], [7].

Due to the fact that different molecules are supposed to be explored with Paultje, it is important to know that in order to trap ions of higher masses, higher rf-voltages are required.

2.4 Electron Cyclotron Resonance Ion Source (ECRIS)

The ion beam used in the experiments is extracted from the Electron Cyclotron Resonance Ion Source (ECRIS). The advantages of this ion source are for one thing the possibility to produce ions out of any element (KVI: any element which can exist in the gas phase) and for another thing no usage of wearing parts. This results in a stable ion beam for a long period, about several days to weeks. The stability of the ion beam is then solely limited by the consumption of the used element. An ECRIS operates in the following way:

Due to the Lorentz-force, electrons in a magnetic field circulate around the magnetic field lines with a frequency $\omega = (e/m)\,x\,B$, where e and m are the electrons charge and mass, respectively, B is the magnetic field. In an ECRIS, this occurs in the plasma chamber in a magnetic bottle between the two solenoids. When microwave radiation of the frequency ω enters the plasma chamber, the electrons are resonantly accelerated and decelerated.

A superposition of axial B-field components with the radial B-field component of the permanent hexapole-magnet results in a minimum-B-structure. This means that the magnetic induction increases from the geometric midpoint of the ion source to the other directions. This results in a closed surface on which the frequency of the applied field is the same as the gyro-frequency of the electrons. There, the heating of the plasma is very efficient. The electrons of the plasma traverse this region very often, gain high energies and ionize atoms and ions of the plasma into high states. Electrons heated at gyro-frequency create a space-charge potential. In the direction of the field-lines of this space-charge potential, the ions are accelerated and extracted. By a system of several magnets, the ions are deflected and focused. Subsequently they are extracted to the experiment, in this case to the Paul trap of the setup.
A schematic view of an ECRIS is shown in fig.6.
In our experiments, He^{+} and He^{2+} ions are extracted from the 14 GHz ECRIS, but there are a lot more possibilities [2], [8].

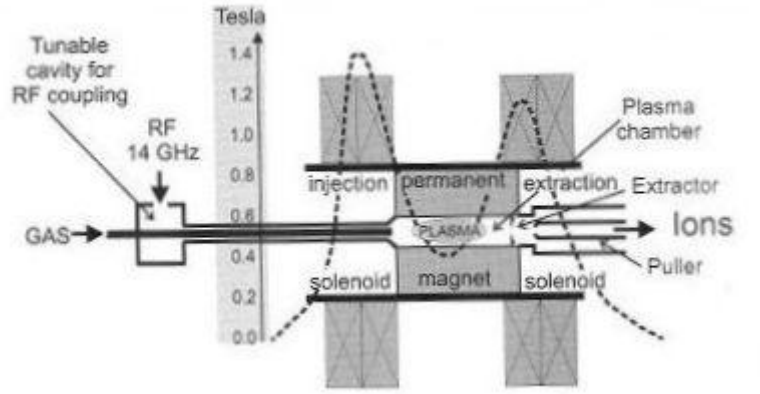

Fig.6: A schematic view of the ECRIS [2].

2.5 Time of Flight mass spectrometry

In a Time of Flight (TOF) Mass Spectrometer, the mass-charge ratio (m/z) of ions is determined by measuring the time it takes for the ions to reach a detector (multichannel plate detector – see section 2.6). The ions are accelerated by an electric field, so that all ions with the same charge get the same kinetic energy (the same velocity). After acceleration, the ions enter a field free flight tube, wherein they are left at a constant velocity. Heavy ions have a longer TOF (lower speeds) than light ions (higher speeds). It can be shown that

$$t \sim \sqrt{m/z} \qquad (2.11)$$

with t the flight time and m/z the mass-charge ratio of the ion.

Equation 2.11 is proven in the appendix.

In the Paultje setup, a linear TOF Mass Spectrometer is used to explore the masses and intensities of the different fragments in which ions decompose after being irradiated with ions from the ECRIS [2], [9].

2.6 Multichannel plate detector

As mentioned before, the ions in the TOF tube are detected by a multichannel plate. A MCP is used for the low-noise amplification of low currents of electrons or other ionizing particles by multiplication of electrons due to secondary emission. The channels of the MCP are not perpendicular to the plate so that entering particles always hit the walls of the channels and start a chain reaction in which many secondary electrons are produced. In this way, the incoming signal is amplified. After being detected, the signal is processed by a computer program (see chapter 4).

2.7 Summary of the experimental setup

To outline the experimental setup, an overview is shown in fig.2.9.

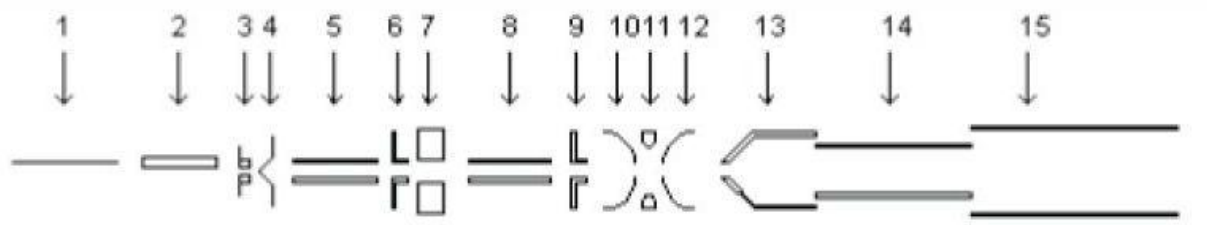

Fig.2.9: An overview of the components [9].

1. Needle (inlet of the electrospray)
2. Capillary
3. Tube lens 1
4. Skimmer
5. Quadrupole (to guide through the ions)
6. Plate 1
7. Plate 2
8. Quadrupole (mass filtering the ions)
9. Tube lens 2
10. entrance Paul trap
11. center Paul trap
12. exit Paul trap
13. Lens 1
14. Lens 2
15. TOF Drift tube with MCP at the end

Chapter 3

Biomolecules

Biomolecules are organic molecules, which appear in living organisms and consist of large polymers (among others proteins, nucleic acids, polysaccharides) and small molecules. In the experiments with the Paultje setup, several biomolecules are used. Some molecules have been extensively studied by other mass-spectrometric techniques, so that the setup can be tested by using these ones (e.g. Leucine-enkephalin, also called leu-enkephalin). Adenosine is one of the molecules which really are of scientific interest, because it is a component of the RNA.

3.1 Leucine-Enkephalin

Leu-Enkephalin is a small peptide consisting of 5 amino-acids (pentapeptide):

Tyr (Tyrosine) – Gly (Glycine) – Gly – Phe (Phenylalanine) – Leu (leucine).

It is produced by the body itself and is neurological pain-relieving.

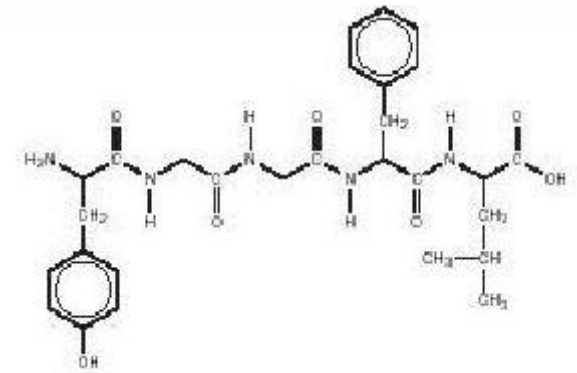

Fig.3.1: Chemical structure of Leu-Enkephalin [10].

Chapter 4

Data acquisition and processing

In this chapter, the software for the Pulse Delay Generator and the data processing with the aid of OriginPro are described.

4.1 Pulse Delay Generator

The Paultje experiment is controlled by a Pulse Delay Generator. With a software, the widths and delays of the extraction, the buffer gas, the ESI, the ion beam and eventually a second pulse of the helium buffer gas are controlled. In this way, many different settings and experiments are possible. One can for example change the width of the ion beam irradiation to study in which way the fragmentation depends on it.

4.2 1GHz Digitizer

The 1GHz Digitizer reads out the temporal process of the detector signal. During a running measurement, a current status of the results is visualized by the Digitizer3In1. On the screen, there are 4 coordinate systems, all of them showing the intensity of ions/fragments against their flight time. The first one shows the result of the current measurement. The second one shows the average result at the ESI source. The third graph is an average of the ions coming from the Paul trap (+background), and the fourth one is for the background itself (also an average). Observing these graphs helps to check whether everything is working as expected. On this screen, the number of measurements for one experiment can be adjusted. For short experiments, a standard value is about 400-500 single measurements per experiment. It is of course useful to increase this number for more accurate results. It is advantageous to perform several experiments of e.g. only 500 acquisitions, and to add them in the end in order to obtain a result with a high signal-to-noise ratio. The advantage of this method in comparison to one single, long-lasting experiment is the possibility to remove single experiments in which experimental problems occur e.g. sudden decrease of the beam current, empty syringe for the electrospray etc. The measurements can be saved by this program and afterwards be imported into OriginPro (see section 4.3).

4.3 (Graphic) Data Processing with OriginPro

Series of measurements can be imported into the computer program OriginPro. The measurements contain information about (detector-) voltages as a function of time for ions

- coming from the ESI source (so without being irradiated yet)
- coming from the Paul trap (after being irradiated), plus the background
- the background

stored in columns B, C, and D, respectively. Column A is used for the flight times.

So $-(c-b-d)$ plotted against the flight time gives information about the loss of the ion of interest (negative peak) and the gain of fragments (positive peaks).

In Chapter 5, these graphs are used to illustrate the experimental results.

Chapter 5

Experiments

In this chapter, the ideas and concepts of the experiments are explained. The expected results are mentioned and subsequently compared with the measured spectra. Note that all experiments were implemented with a second pulse of the helium buffer gas and a liquid nitrogen cooling (LN_2).

5.1 Probability of multiple collisions depending on the ion flux

In a first series of experiments, fragmentation of the peptide Leu-enkephalin due to collisions with keV ions was observed. This section focuses particular on the probability of multiple collisions and differences in the irradiation time.
For a low ion-flux, smaller relative fragment yield is expected. The amount of remaining unaffected leu-enkephalins should be nearly as large as before the irradiation. For a higher ion-flux, we expect larger relative fragment yield, due the fact that for a higher flux, the probability is higher that a He^{2+} collision with a leu-enkephalin molecule occurs. The amount of unaffected leu-enkephalin molecules after irradiation should certainly be less than before irradiation. We keep the ion-flux constant and vary only the duration of the irradiation to change the number of ions in the beam.

In the next section, the probability of double dissociation is calculated for the present experimental circumstances.

5.2 Theoretical probability of double dissociation

To calculate the probability for a leu-enkephalin molecule to dissociate, the number of He^{2+} ions coming from the ECRIS per unit of time has to be calculated. Assuming that the current is 50nA, the number of He2+ ions can be calculated as follows:

$$50nA = 50\frac{nC}{s} \qquad (5.1)$$

The charge of one He^{2+} ion is 2e, as two electrons are missing.

$$2e = 2 * 1.6 * 10^{-19}C = 3.2 * 10^{-19}C \qquad (5.2)$$

The number of He^{2+} ions coming from the ECRIS per second is calculated by

$$\#He^{2+} * 3.2 * 10^{-19}C = 50\frac{nC}{s} \qquad (5.3)$$

$$\Leftrightarrow \quad \#He^{2+} = 1.5625 * 10^{11}\, s^{-1} \qquad (5.4)$$

Additionally, it is assumed that the irradiated surface (≙ surface of the hole in the Paul trap for the incoming ion beam) of the Paul trap is $A = 1mm * 1mm = 10^{-6}m^2$, and that there are $N = 10000$ leu-enkephalin molecules in the trap. For collision induced dissociation, it was found that the cross-section for leu-enkephalin is $\Omega = 162Å^2$ [11]. The number of hit leu-enkephalins in the trap during an irradiation time of 1s is

$$\#^{leu-enk} = \#He^{2+}\,\frac{N * \Omega}{A} = 1.5625 * 10^{11} * 10000 * \frac{162Å^2}{10^{-6}m^2} \simeq 2531 \qquad (5.5)$$

So that the probability for one leu-enkephalin molecule to be hit by a He^{2+} is about 25.3%, since there are totally $N = 10000$ target molecules in the trap.

The probability for double dissociation is determined by the infinite geometric series [12]:

$$\sum_{k=0}^{\infty} r^k = \frac{1}{1-r} \qquad (5.6)\,,$$

with $r = 25.3\% = 0.253$.

The probability for at least double dissociation is

$$\sum_{k=2}^{\infty} 0.253^k = \sum_{k=0}^{\infty} 0.253^k - \sum_{k=0}^{0} 0.253^k - \sum_{k=1}^{1} 0.253^k$$

$$= 1.339 - 1 - 0.253$$

$$= 0.086.$$

The ratio of the single and double dissociated molecules is

$$\frac{0.086}{0.253} = 0.34 = 34\%$$

This means that 34% of the dissociated molecules dissociated twice. This falsifies the experiments immensely, because only once dissociated molecules are supposed to be measured. In order to decrease the distortion, it is made sure that the loss of leu-enkephalin molecules is in the order of 10%. In this way, the ratio of single and double dissociated molecules is decreased:

It is given that:

$$\sum_{k=1}^{\infty} r^k = 10\% = 0.1$$

Since

$$\sum_{k=0}^{\infty} r^k = \frac{1}{1-r} \qquad and \qquad \sum_{k=1}^{\infty} r^k = \sum_{k=0}^{\infty} r^k - 1 \quad ,$$

r is calculated by

$$0.1 = \frac{1}{1-r} - 1 \qquad \Rightarrow r \cong 0.09.$$

Now, the series can be calculated:

$$\sum_{k=1}^{\infty} r^k = \sum_{k=0}^{\infty} r^k - 1 = \frac{1}{1-0.09} - 1 = 0.0989$$

$$\sum_{k=2}^{\infty} r^k = \sum_{k=0}^{\infty} r^k - 1 - 0.09 = \frac{1}{1-0.09} - 1 - 0.09 = 0.0089$$

This results in a ratio of

$$\frac{0.0089}{0.0989} \cong 0.09 = 9\% \quad ,$$

so only 9% of the dissociated molecules dissociated twice.

5.3 Results

For this experiment, among others a He^{2+} beam of 20kV was used. The lowest He^{2+} flux was $1{,}5625 * 10^{10} \frac{1}{0.1s}$, the highest He^{2+} flux was $9.375 * 10^{10} \frac{1}{0.6s}$ (corresponding to irradiation times of 0.1s and 1.6s, respectively). To illustrate what globally happens when the irradiation time is increased, these two spectra are compared in fig.5.1a and b. Note that the loss of leu-enkephalin molecules is set to -1, so that the intensity of the fragments can be seen as relative intensities, which makes a comparison easier.

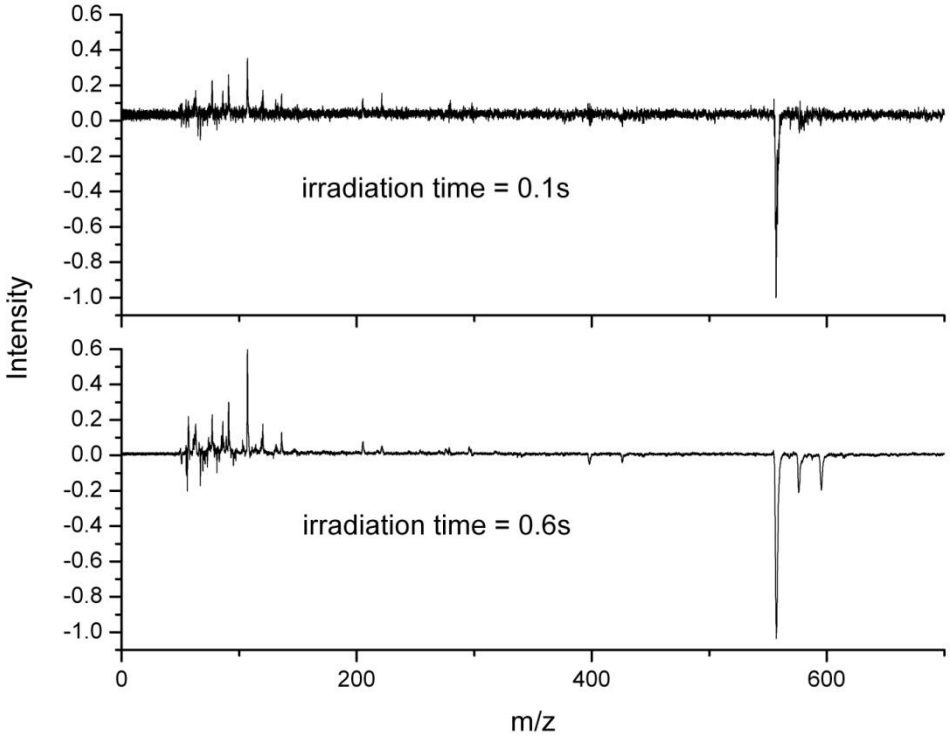

Fig.5.1a: A mass spectrum of leucine-enkephalin irradiated with 20kV He^{2+} with different irradiation times.

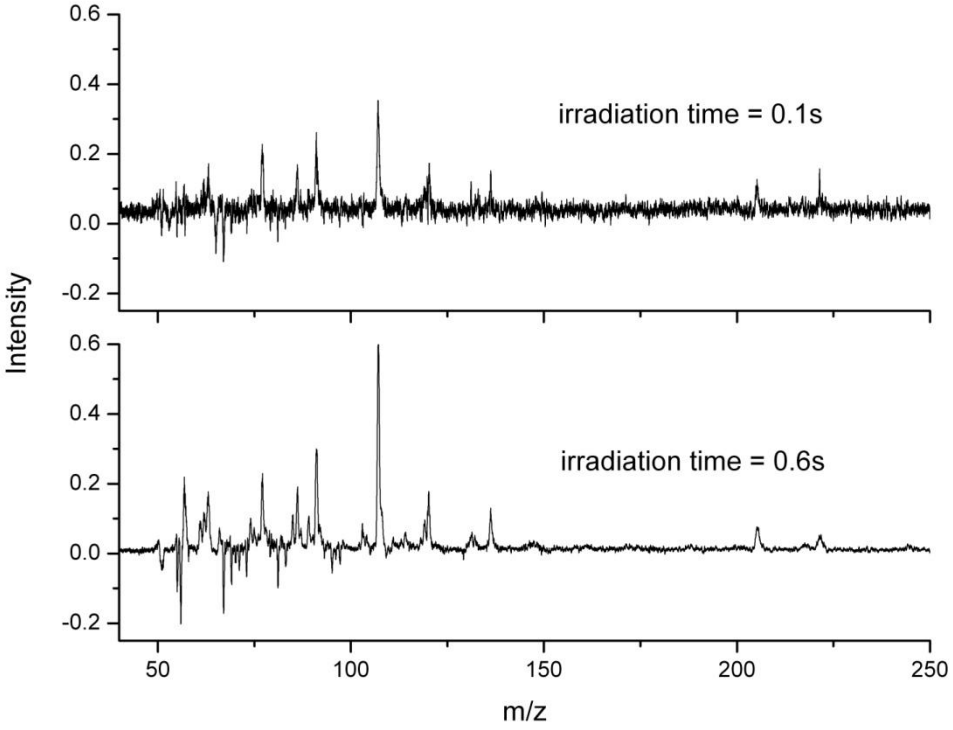

Fig.5.1b: A magnification of the essential part of the spectrum.

It is easy to see that the intensity of most of the peaks is higher for ω = 0.6s. Taking a closer look, you see that for lower masses (57 Da – 107 Da), the intensities are always higher for ω = 0.6s, But for higher masses (120 Da and 136 Da), the intensities are equal or slightly less for ω = 0.6 compared to ω = 0.1. An assumption is that double dissociation takes place and that large fragments could collide with He2+ projectiles, too, which is more probable for longer irradiation times. If they fragment again, the amount of high-mass fragments decreases and the amount of low-mass fragments increases.

5.4 Fragmentation of leu-enkephalin for different keV projectile ions

Another idea is to use projectiles of different voltages. In our experiment, we use He^{2+} ions of 5kV and 20kV. The aim is to find out about the difference in fragmentation of leucine-enkephalin depending on the kinetic energy of the projectiles. Intuitively, higher kinetic energy should result in a higher intensity of the fragments and perhaps even in additions fragment which don't occur at low kinetic energies.

5.5 Results

In order to compare the effect on fragmentation due to changing velocities, two spectra are measured with the same irradiation time ω = 0.2s. The result is shown in fig.5.2a and b.

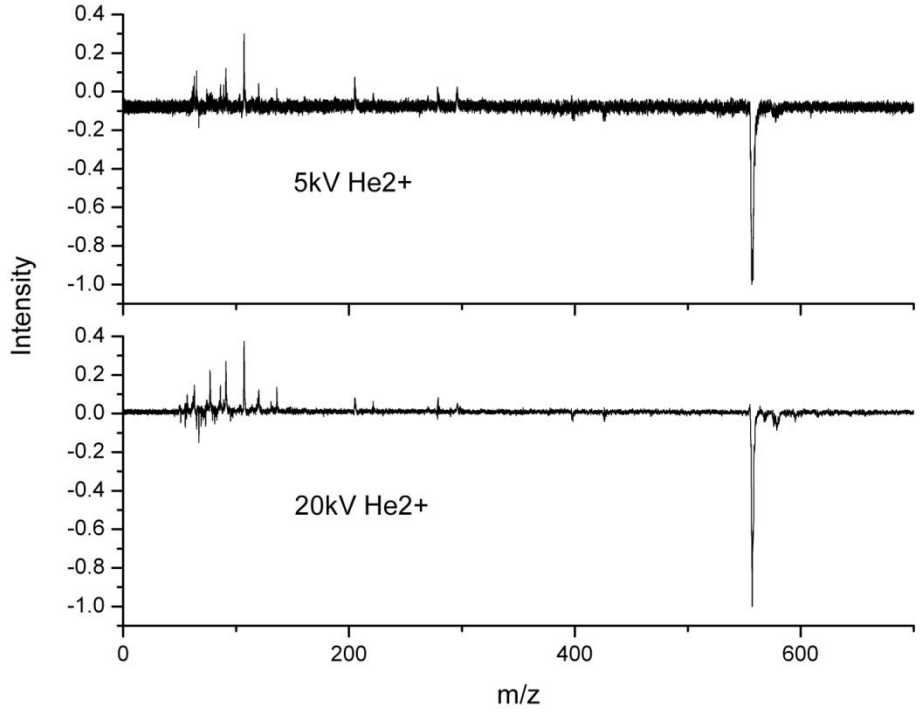

Fig.5.2a: A mass spectrum of leucine-enkephalin irradiated with projectiles at different kinetic energies.

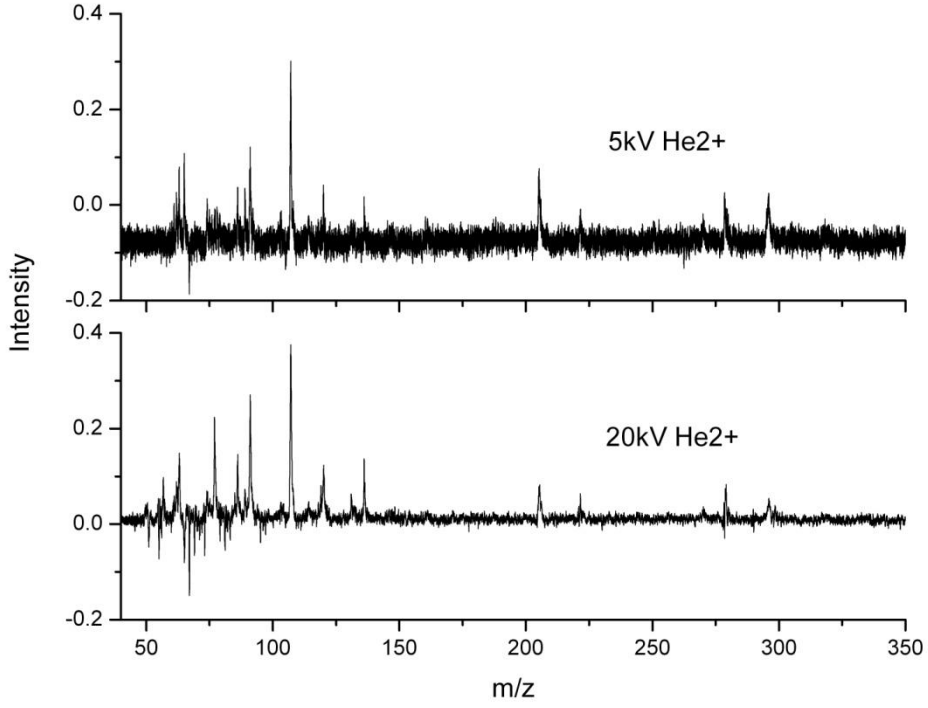

Fig.5.2b: A magnification of the low masses of the spectrum.

Using the 20kV projectiles, the intensity of the 107 Da fragments is approximately 1.5 times higher and for 91 Da, the intensity is even about 2.6 times higher compared to the intensities for the 5kV projectiles. This can be explained by the electronic stopping power. Due to the inelastic collisions between electrons in the leu-enkephalin molecule and the projectile ion, the projectile ion looses energy on a certain path length depositing this energy in excitation energy of the electrons. For keV ions, electronic stropping is a kind of friction force which decelerates the projectile ions. So electronic stopping can be written as

$$S(E) = -\frac{dE}{dx} = -\gamma * v \qquad (5.7)$$

with E the energy, x the path length, γ the friction coefficient (depends on the electrons density in the molecule) and v the projectile ion velocity.

From equation 5.7 it can be seen that

$$S(E) \sim v \sim \sqrt{E} \qquad (5.8)$$

The electronic stopping power is proportional to the velocity of the projectile and to the square root of its energy. For higher velocities, the He^{2+} ions deposited more energy in the electrons of the leu-enkephalin molecules, and therefore produced more fragments.

Fragments of 76 Da and 63 Da only appear when 20kV He2+ ions are used. Fragments of 65 Da solely appear in the spectrum used the 5kV ions.

Faster projectiles produce more heavy fragments than slow projectiles. It is interesting, that only at 5kV fragments of 65 Da, and only at 20kV fragments of 63 Da are produced. It could be a prospective task to find out whether this is due to inaccuracy (because of the small number of acquisitions) or whether this is a reproducable effect.

5.6 Dissociation of leu-enkephalin depending on the charge of the projectile

Another idea is to find out about the dependence on the charge of the projectiles. Using He+ ions at 20kV and He2+ ions at 10kV, it is made sure that the projectiles have the same velocities, but different charges. We choose an irradiation time of 0.15s. Measured spectra are shown in fig.3a and b.

5.7 Results

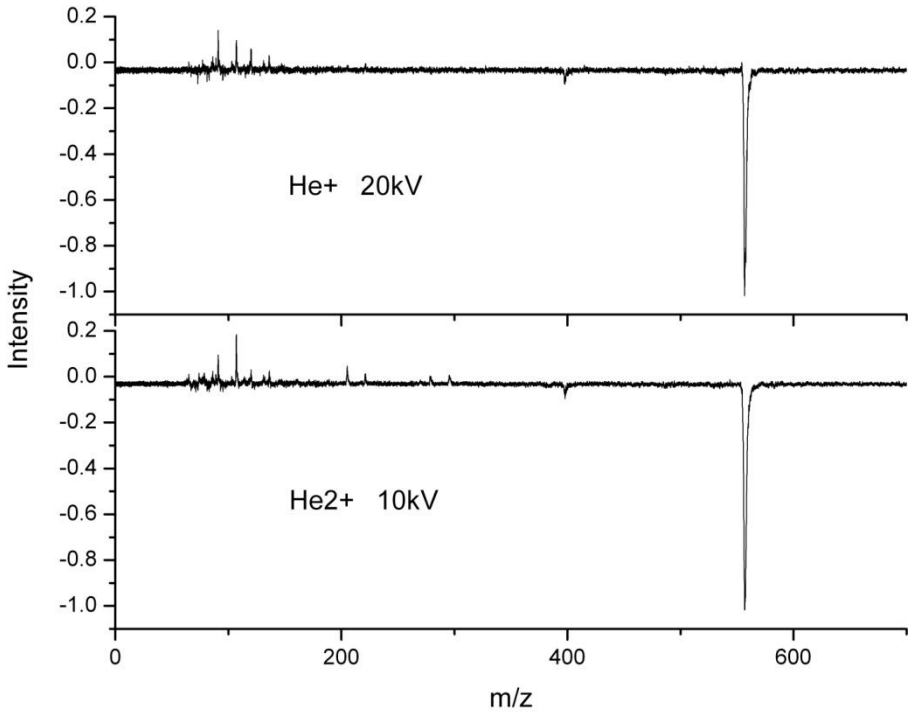

Fig.5.3a: A mass spectrum of the fragmentation of leucine-enkephalin with differently charged projectiles.

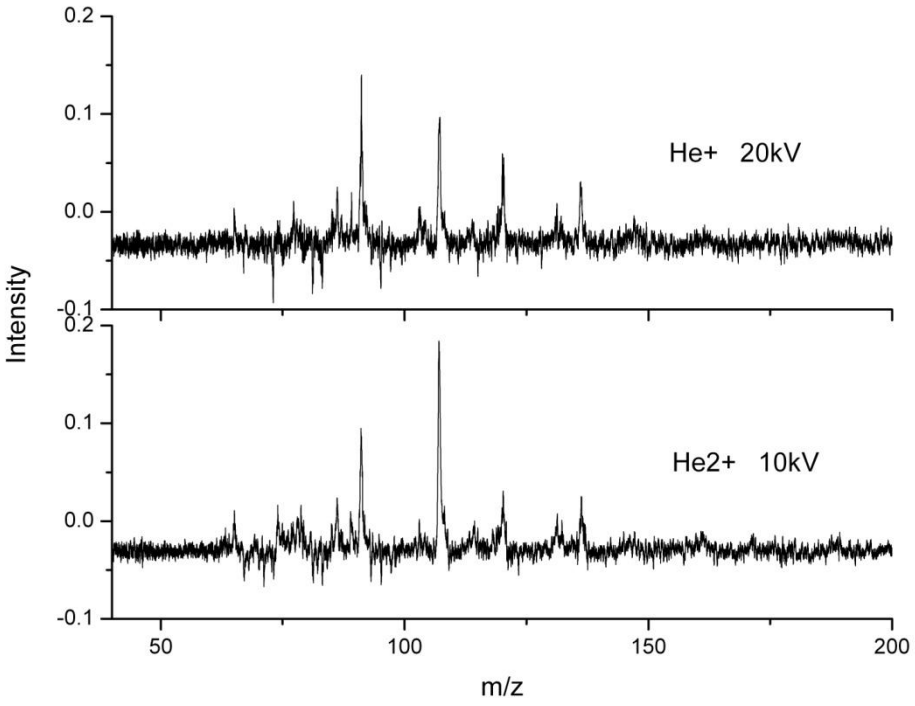

Fig.5.3b: A more precise view on the the originated fragments.

The intensities of the 136 Da fragments are even high for both cases, but the amount of the 120 Da fragments is more than twice as high using single charged ions. Also for the 91 Da fragments, the intensity is 0.5 times higher for the single charged ions compared to the intensity for the double charged ions. Only for the fragments of mass 107 Da, the intensity became twice as high using double charged ions.

Theoretically, it is assumed that resonant charge capture takes place at the HOMO of the leucine-enkephalin molecule (of the order 10eV). A He^+ ion can capture one electron in the first (n=1) shell (~25eV), capturing in the second (n=2) shell is at ~5eV. But 10eV of the HOMO is neither resonant to 25eV, nor to 5eV, what makes resonant charge capture improbable.
For He^{2+} ions, the first shell is stronger bound than for He^+, but resonant charge capture is here improbable, too. But the n=2 shell is bound at ~12eV, hence resonant charge capture is possible because this is resonant with states below the HOMO of leu-enkephalin. This is what physically makes the difference between the two measured spectra.

It is obvious that the charge of the projectiles affects the fragmentation on leu-enkephalin. Due to the fact that there is no clear trend recognizable in these measurements, they should be repeated with a larger number of acquisitions and with some other irradiation times.

Chapter 7

Useful improvements of Paultje

There are several improvements of the Paultje setup which were done during my Bachelor Project at the KVI, and which are planned to be done in the future.

The octupole mass filter is replaced by a quadrupole mass filter because of better control and filtering properties.

A new voltage source was made for the detector of the TOF mass spectrometer, which makes sure that the voltage difference can't become too high. A high voltage difference would destroy the detector.

A new cooling arrived which will replace the liquid nitrogen cooling in the future. Lower temperatures will be reached, so that more uncharged molecule can be "frozen" on the cooling plate in the setup. This will result in a lower background.

It is planned to place a lens between the mass filter and the Paul trap, so that ions get focused and less of them get lost.

Moreover, it would be advantageous to use a Reflectron TOF instead of a linear TOF. In a Reflectron TOF, higher energy ions enter deeper into the reflectron, so that their paths are longer. The paths of lower energy ions are shorter. This would improve the resolution compared to a linear TOF.

Finally, the whole setup could be propped on a more robust framework. Paultje consists of a lot of heavy components lying on a –compared to the setup- unfirm framework. It is assumed that this is the reason for inaccuracies with regard to the ion beam entering the Paul trap and the necessity for the re-alignments which were done.

Chapter 8

Appendix

Chapter 2.2

Equations of motion

Ions in a quadrupole field experience restoring forces that drive them back toward the center of the trap. The motion of the ions in the field is described by the solutions to the Mathieu equation. When written for ion motion in a trap, the equation is

$$\frac{d^2u}{d\xi^2} = [a_u - 2q_u cos(2\xi)]u = 0 \qquad (1)$$

where u represents the x, y and z coordinated, ξ is a dimensionless parameter given by $\xi = \frac{\Omega t}{2}$, and a_u and q_u are dimensionless trapping parameters. The parameter Ω is the radial frequency of the potential applied to the ring electrode. By substituting the expression for ξ into Equation 1, one obtains

$$4\frac{d^2u}{d\Omega^2 t^2} + (a_u - 2q_u \cos(\Omega t))u \qquad (2)$$

$$m\frac{d^2u}{dt^2} = -m\frac{\Omega^2}{4}(a_u - 2q_u \cos(\Omega t))u \qquad (3)$$

By Newton's laws of motion, the above equation represents the force on the ion. The forces in each dimension are not coupled, thus the force acting on an ion in, for example, the x dimension is

$$F_x = ma = m\frac{d^2x}{dt^2} = -e\frac{\partial\phi}{\partial x} \qquad (4)$$

Here, ϕ is the quadrupolar potential, given by

$$\phi = \frac{\phi_0}{2r_0^2}(\lambda x^2 + \sigma y^2 + \gamma z^2) \qquad (5),$$

where ϕ_0 is the applied electric potential and λ, σ, and γ are weighting factors, and r_0 is a size parameter constant, more precisely half the distance between two opposite electrodes. The Laplace Condition, $\nabla^2\phi_0 = 0$, which holds in any electric field, causes the requirement

$$\lambda + \sigma + \gamma = 0 \qquad (6).$$

For a quadrupole mass filter, $\lambda = -\gamma = 1$ and $\sigma = 0$. For an ion trap, $\lambda = \sigma = 1$ and $\gamma = -2$.

First, the trapping parameters for the mass filter will be calculated. Equation 5 becomes

$$\phi = \frac{\phi_0}{2r_0^2}(x^2 - z^2) \qquad (7)$$

The applied electric potential, a combination of a r.f. and a dc signal, is given by

$$\phi_0 = U + Vcos(\Omega t) \qquad (8)$$

With $\Omega = 2\pi\upsilon$, where υ is the applied frequency in Hertz.

Differentiating equation 7 with respect to x and substituting equation 8 yields

$$\frac{\partial\phi}{\partial x} = \frac{x\,\phi_0}{r_0^2} = \frac{x}{r_0^2}\big(U + Vcos(\Omega t)\big) \qquad (9)$$

Substituting this into equation 4 gives

$$F_x = -e\frac{x}{r_0^2}\big(U + Vcos(\Omega t)\big) \qquad (10)$$

Replacing u by x in equation 3, you get

$$m\frac{d^2x}{dt^2} = -m\frac{\Omega^2}{4}(a_x - 2q_x\cos(\Omega t))x \qquad (11)$$

Both equations 10 and 11 represent a force on an ion, so the right hand sides are equal. By comparison it is easily to see that

$$-eU\frac{x}{r_0^2} = -mx\frac{\Omega^2}{4}\,a_x \qquad and \qquad -eVcos(\Omega t)\frac{x}{r_0^2} = mx\frac{\Omega^2}{4}\,2q_x\cos(\Omega t) \qquad (12)$$

Rearranging gives

$$a_x = \frac{4eU}{r_0^2 m\Omega^2} \qquad and \qquad q_x = -\frac{2eV}{r_0^2 m\Omega^2} \qquad (13)$$

Because of the weighting constants $\lambda = -\gamma = 1$, a_z and q_z are given by $-a_x$ and $-q_x$, respectively.

Chapter 2.3

For the ion trap ($\lambda = \sigma = 1$ and $\gamma = -2$), this calculation is nearly similar to that above. The only difference is caused by the different weighting constants and equation 5 becomes

$$\phi = \frac{\phi_0}{2r_0^2}(x^2 + y^2 - 2z^2) \qquad (14)$$

Differentiating equation 14 with respect to x and substituting equation 8 gives

$$\frac{\partial \phi}{\partial x} = \frac{x\phi_0}{r_0^2} = \frac{x}{r_0^2}\big(U + Vcos(\Omega t)\big) \qquad (15)$$

Again,

$$F_x = -e\frac{\partial \phi}{\partial x} = -e\frac{x}{r_0^2}\big(U + Vcos(\Omega t)\big) = -m\frac{\Omega^2}{4}(a_x - 2q_x\cos(\Omega t)) \qquad (16)$$

This yields to the same comparison as equation 12 calculated for the mass filter. From here, the derivation of the trapping parameters of the ion trap is precisely the same as for the mass filter, and, of course, the same results for a_x and q_x are obtained (eq.13). For the ion trap, $\lambda = \sigma = 1$, so $a_x = a_y$ and $q_x = q_y$.
The force in the *z*-direction is calculated by differentiating equation 14 with respect to *z*:

$$\frac{\partial \phi}{\partial z} = -\frac{2z}{r_0^2}\phi_0 = -\frac{2z}{r_0^2}(U + Vcos(\Omega t)) \qquad (17)$$

$$F_z = -e\frac{\partial \phi}{\partial z} = \frac{2ez}{r_0^2}\big(U + Vcos(\Omega t)\big) \qquad (18)$$

The Mathieu equation yields

$$F_z = m\frac{d^2z}{dt^2} = -m\frac{\Omega^2}{4}(a_z - 2q_z\cos(\Omega t))z \qquad (19)$$

Comparing 18 and 19 and rearranging gives

$$a_z = -8\frac{eU}{r_0 m\Omega^2} \qquad and \qquad q_z = 4\frac{eV}{r_0 m\Omega^2} \qquad (20)$$

Chapter 2.5

The potential energy of a charged particle in an electric field is given by

$E_{pot} = qU$ (21)

With q the charge of the particle and U the electric potential.

Due to the voltage U, the particle accelerates and its kinetic energy increases. The kinetic energy is known as

$E_{kin} = \frac{1}{2} m v^2$ (22)

During the acceleration of the particle due to the voltage U, the potential energy is converted to kinetic energy, so these energies are equal, resulting in

$E_{pot} = E_{kin}$ (23)

$qU = \frac{1}{2} m v^2$ (24)

After acceleration, the charged particle has a constant velocity, because there is no electric field anymore which would accelerate it. This velocity can easily be calculated by the fact that velocity is equal to path / time :

$v = \frac{d}{t}$ (25)

With d the length of the TOF tube.

Substituting equation (25) in (24) yields

$qU = \frac{1}{2} m \left(\frac{d}{t}\right)^2$ (26)

$\Rightarrow t = \frac{d}{\sqrt{2U}} \sqrt{\frac{m}{q}}$ (27)

Since d and U are constant, equation (27) can be expressed as

$t \sim \sqrt{\frac{m}{q}}$ (28)

The time of flight of a charged particle changes with the square root of its mass/charge ratio.

Chapter 9

Acknowledgements

I want to thank drs. Sadia Bari for the opportunity to take part in a fascinating experiment and for answering all my questions so patiently. I do not regret the choice of the experiment and that I have been there for such a long time – in this way I have seen how the experiment developed in this period. I also want to thank dr. Thomas Schlathölter for the ideas and hints for my bachelor thesis. I'm grateful for the supervision by prof. dr. ir. Ronnie Hoekstra.

I enjoyed the atmosphere in the atomic physics group and I would recommend to any student, who is interested in it, to do their projects in this group.

Bibliography

1. David Secko, *A Monk's Flourishing Garden: The Basics of Molecular Biology explained,* The Science Creative Quartely of the University of California, Berkeley, 2003
http://www.scq.ubc.ca/a-monks-flourishing-garden-the-basics-of-molecular-biology-explained/

2. Fresia Alvarado Chacón, *Ion induced radiation damage on the molecular level*, Proefschrift, 2007

3. S.J. Gaskell, *Electrospray: principles and practice,* Journal of Mass Spectrometry, 32: 677-688, 1997

4. John B. Fenn et al, *Electrospray Ionization for Mass Spectrometry of Large Biomolecules,* Science, 246: 64-71, 1989

5. Roel H. Fokkens, *Mass Spectrometric Methods in Biomolecular Structure Elucidation*, 6-10, 2002

6. Wolfgang Paul, *Electromagnetic traps for charged and neutral* particles (Nobel lecture), 1989

7. Raymond E.March, *An introduction to quadrupole ion trap mass spectrometry*, Journal of Mass Spectrometry, 32: 351-369, 1997

8. L.C.J.M. De Kock, *Experimental Study of Ion Heating by Wave Mixing in an Electron-Cyclotron-Resonance Plasma,* 6-7, 1973

9. Femke van Seijen, *Mass Spectrometry of Biomolecules using electrospray ionization and a quadrupole ion trap*, Bachelor thesis, 2008

10. V. Stefanovich, I. Okyayuz-Baklouti, *Role of Adenosine in Cerebral Metabolism And Blood Flow*, 1, 1987

11. Nick C. Polfer et al, *On the Dynamics of Fragment Isomerization in Collision-Induced Dissociation of Peptides,* J. Phys. Chem., 112: 1286-1293, 2008

12. http://mathworld.wolfram.com/GeometricSeries.html